# Probability Density Function Approach for Multidimensional Turbulent Flow Calculations with Application to In-Cylinder Flows in Reciprocating Engines

Daniel C. Haworth* and Sherif H. El Tahry†
*General Motors Research Laboratories, Warren, Michigan 48090*

**The probability density function (pdf) method is extended to two- and three-dimensional transient turbulent flows. The numerical approach couples a Lagrangian Monte Carlo method to solve for the joint pdf of velocity and scalar compositions with an Eulerian finite-volume algorithm to calculate mean pressure and a turbulence time scale. A general approach applicable to variable-density chemically reacting flows has been taken; the present results are for nearly uniform density inert flows. Three engine-like configurations have been investigated: 1) a noncompressing axisymmetric cylinder-piston assembly with a central port; 2) a noncompressing axisymmetric cylinder-piston assembly with an annular port; and 3) a compressing three-dimensional configuration with an off-center valve. Pdf results are compared with measurements and with conventional $k$-$\epsilon$ calculations for the two axisymmetric geometries. For these noncompressing flows the pdf approach is found to have little advantage over a $k$-$\epsilon$ model. Mean velocity profiles from both models are in good agreement with experiment for the central port case, whereas agreement for the annular port is less satisfying. Root-mean-square axial velocities from both models are low at early times in the intake process, but improve later in the cycle. Influence of numerical parameters on solution accuracy is assessed. The present work confirms the feasibility of the pdf approach for complex turbulent flows and represents an intermediate step in the application of pdf methods to multidimensional turbulent reacting flows, where they are expected to offer their greatest advantage.**

## I. Introduction

MULTIDIMENSIONAL modeling is emerging as an important diagnostic/design tool for in-cylinder flows in reciprocating engines. Recent work includes studies of flow structure, mixing, and turbulence in nonreacting flows[1,2]; simulations of combustion in homogeneous-charge spark ignition engines[3,4]; and studies of sprays and combustion in direct-injection spark ignition[5,6] and Diesel[7] engines. These studies serve to validate submodels and numerical algorithms, increase insight into the nature of the physical process occurring inside the engine cylinder, and provide guidance for design. Although at least qualitative agreement with experiment often is achieved (when data are available), both physical modeling uncertainties and numerical difficulties pose formidable obstacles to the development of truly predictive simulations. Physical complexities requiring modeling include turbulence, chemical reaction (including ignition and pollutant formation), multiphase flows (i.e., fuel sprays), wall effects, and interactions among these phenomena. The transient three-dimensional nature of the flowfield, moving boundaries, and wide ranges of physically important length and time scales complicate the numerical algorithms. Thus, in using the simulations one is obliged not to stray far from the conditions under which the models have been calibrated: The development of improved physical submodels and numerical algorithms remains an important task in realizing the full potential of multidimensional modeling as a quantitative, predictive tool for engine design.

Turbulence models used in multidimensional modeling studies of in-cylinder flows typically have been of either the constant diffusivity or two-equation (e.g., $k$-$\epsilon$) variety[1-9] ($k$ being the turbulent kinetic energy and $\epsilon$ its viscous dissipation rate). There have been few attempts to apply higher-order closures to complex turbulent flows; an exception is the work of El Tahry,[9] who applied the Reynolds stress model of Launder et al.[10] to the annular intake flow considered in the present study.

Two widely used models for the mean conversion rate of reactants to products in engine combustion are "chemically controlled" models, where the reaction time scale is determined by an Arrhenius expression relating mean reaction rate to mean concentrations and temperature,[3,5,7,11] and "mixing-controlled" models, where the time scale of the reaction is proportional to the turbulence time scale $\tau = k/\epsilon$.[12] The former are inappropriate extensions of the instantaneous laminar combustion rate expression to the mean turbulent reaction rate, whereas the latter are valid only when the chemical time scale is shorter than the turbulence time scale $\tau$. Hybrid schemes that allow either kinetics or mixing to become rate controlling have been applied in a number of engine modeling studies.[4,6,13] Flamelet models[14] are another approach that has shown promise for homogeneous-charge engine combustion.

Probability density function (pdf) methods provide an alternative approach to turbulence and turbulent combustion modeling that requires fewer modeling assumptions and hence, in principle, should be more accurate and general. In the pdf method we solve for the joint pdf of either the scalar composition variables defining the thermochemical state of the system (composition pdf) or the scalar compositions plus the three components of velocity (velocity-composition pdf). Closure problems associated with strongly nonlinear chemical reaction rates and (for the velocity-composition pdf) with the mean pressure gradient, body forces, and convective transport are overcome. Molecular transport and the fluctuating pressure gradient remain to be remodeled.

Composition pdf approaches have been applied to engine flows by Brandstätter and Johns[15] and by Borghi et al.[16,17] In all cases two-equation turbulence models have been used together with gradient transport assumptions. Such assumptions undermine the performance of the model, particularly in

---

Received Nov. 13, 1989; revision received Feb. 26, 1990. Copyright © 1990 by the American Institute of Aeronautics and Astronautics, Inc. All rights reserved.

*Senior Research Engineer, Thermosciences Department.

†Senior Staff Research Engineer, Thermosciences Department.

premixed flames with high density ratios where countergradient diffusion has been shown to be important.[18] The velocity-composition pdf formulation used in the present work avoids gradient diffusion models; the modern foundations for this approach can be found in the papers of Lundgren[19] and Pope.[20]

Because of their large dimensionality ($7+\sigma$ independent variables for the joint pdf of velocity and $\sigma$ scalar compositions in three spatial dimensions and time), pdf transport equations are not amenable to solution by conventional numerical techniques; Monte Carlo algorithms have been developed as an alternative.[20,21] Lagrangian solution procedures are used in contrast to the Eulerian formulation that is the basis for most alternative methods.

Examples of modeling studies using the velocity-composition pdf and Monte Carlo solution algorithm may be found in Refs. 22–27. Until recently, these applications had been limited to relatively simple flow configurations (i.e., statistically one-dimensional transient, two-dimensional boundary-layer, and self-similar flows), including both premixed flames[24] and diffusion flames.[25] Anand et al.[26] have extended the method to incompressible statistically stationary two-dimensional elliptic flows by coupling the Monte Carlo method to a finite-volume calculation for the flow over a backward-facing step. Here we follow a similar coupled approach with an algorithm appropriate for transient two- and three-dimensional variable-density flows. Some results for an axisymmetric engine-like configuration have been reported by Haworth and El Tahry.[27] The present work expands on the results presented in Ref. 27, provides details of the modeling and numerical method including studies of numerical errors, and reports the first three-dimensional results obtained via the velocity-composition pdf method.

The next section contains a review of the pdf method for turbulent reacting flows. Section III describes the flows to be investigated. The numerical methods and modeling are presented in Sec. IV; this includes the finite-volume algorithm and $k$-$\epsilon$ turbulence model and the Monte Carlo algorithm with its associated models. Section V contains the results. The Monte Carlo results are evaluated with respect to measurements and to $k$-$\epsilon$/finite-volume calculations; the sensitivity of results to the choice of numerical parameters is presented. And finally, results are summarized and conclusions are drawn.

## II. Probability Density Function Method

The goal of the velocity-composition pdf method is to determine the evolution of the one-point joint probability density function of the velocities $\underline{U}(\underline{x},t)$ and of the $\sigma$ scalars $\underline{\phi}(\underline{x},t)$ describing the thermochemical state of the system (i.e., species mass fractions and enthalpy). The joint pdf $\tilde{f}_{\underline{U}\underline{\phi}}(\underline{V},\underline{\psi};\underline{x},t)$ is the mass-weighted probability density of the event $\{\underline{U}(\underline{x},t)=\underline{V},\underline{\phi}(\underline{x},t)=\underline{\psi}\}$. This pdf is a density in the $3+\sigma$ dimensional velocity-composition space; it is also in general a function of position $\underline{x}$ and of time $t$.

All one-point statistics of any function of the velocities and compositions $Q(\underline{U},\underline{\phi})$ can be expressed as probability-weighted integrals. The density-weighted mean, or Favre average, of $Q$ is denoted by a tilde:

$$\tilde{Q}(\underline{x},t) = \iint Q(\underline{V},\underline{\psi})\tilde{f}_{\underline{U}\underline{\phi}}(\underline{V},\underline{\psi};\underline{x},t)\,\mathrm{d}\underline{V}\,\mathrm{d}\underline{\psi} \tag{1}$$

where the integration is over the entire velocity-composition space. The conventional average (denoted by angled brackets $\langle\ \rangle$) can be expressed similarly.[20] Fluctuations with respect to the conventional mean are denoted by a single prime (except for velocity, where lowercase $\underline{u}$ is used), whereas two primes are used for fluctuations with respect to the density-weighted mean. Thus, for example, the density-weighted Reynolds stress tensor can be written as (in Cartesian tensor notation)

$$\widetilde{u_i''u_j''}(\underline{x},t) = \iint [V_i - \tilde{U}_i(\underline{x},t)][V_j - \tilde{U}_j(\underline{x},t)] \times \tilde{f}_{\underline{U}\underline{\phi}}(\underline{V},\underline{\psi};\underline{x},t)\,\mathrm{d}\underline{V}\,\mathrm{d}\underline{\psi} \tag{2}$$

where $\tilde{U}_i$ is obtained from Eq. (1) with $Q(\underline{U},\underline{\phi}) = U_i$. The dependence of mean variables on $\underline{x}$ and $t$ is henceforth dropped. For uniform density flows such as those being considered in the present study, Favre and conventional averages are identical; then $\tilde{U}_i = \langle U_i \rangle$, $\widetilde{u_i''u_j''} = \langle u_i u_j \rangle$, etc.

The integro-differential equation governing the evolution of the joint pdf is derived from the Eulerian conservation equation for mass, momentum, and scalar compositions.[20] In this pdf transport equation, terms representing convective transport, the mean pressure gradient, body forces, and reaction source terms appear in closed form even in variable-density flows, whereas terms representing molecular transport and the fluctuating pressure gradient require modeling. The pdf method proceeds by modeling these terms and solving the pdf transport equation; the numerical solution is accomplished using Monte Carlo methods.

A Lagrangian approach has proven to be fruitful for modeling and solving pdf equations for turbulent flows[20–27]: We model the behavior of fluid particles using "notational" particles whose motion in the $6+\sigma$ dimensional position-velocity-composition state space is governed by stochastic processes. These stochastic models plus information on turbulence length or time scales effectively provide closure models for the terms involving molecular transport and the fluctuating pressure in the pdf transport equation.

## III. Flows

Two axisymmetric engine-like flows are selected to test the new modeling approach. The chamber configuration is a pancake (flat head and piston) cylinder with a 75-mm bore,

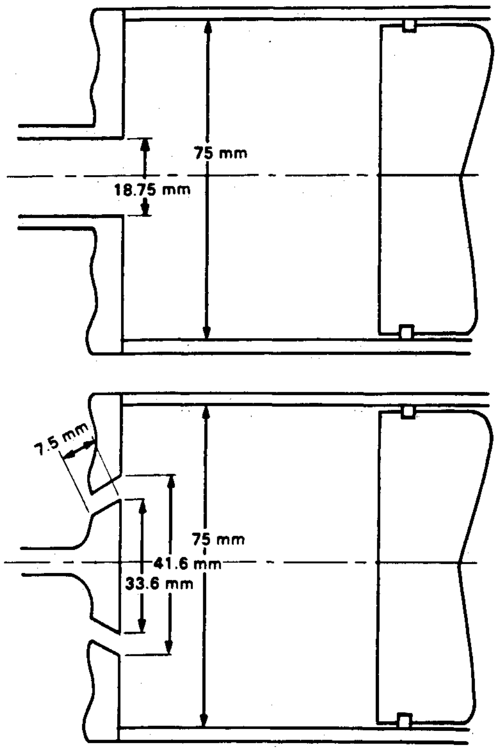

**Fig. 1 Axisymmetric piston-cylinder assemblies, with central port (top) and annular port (bottom).**

60-mm stroke, and 30-mm clearance (Fig. 1). There is no compression: The piston is driven in simple harmonic motion at a speed of 200 rpm (mean piston speed $\bar{V}_p = 0.4$ m/s), and the inlet/exhaust port remains open throughout the stroke. The two flows differ only in the port configuration.

For the first case flow enters the chamber through a central pipe of length 1.8 m. The second arrangement consists of a centered annular port simulating an open valve: The annulus is angled at 30 deg with respect to the cylinder axis. For both flows laser-Doppler anemometry has been used to obtain radial profiles of mean and rms axial velocity at 10-mm axial increments starting from the head for crank angles of 36, 90, 144, and 270 deg after top dead center.[28]

Several sets of earlier $k$-$\epsilon$ calculations are available for these axisymmetric flows.[9,29,30] Gosman et al.[29] report for both the central and annular ports; El Tahry[9] and Diwakar and El Tahry[30] present calculations for the annular port. Reference 9 includes systematic studies of the effects of grid refinement, differencing techniques (quadratic vs skew upwind), and turbulence models (constant diffusivity vs $k$-$\epsilon$ vs Reynolds stress).

Demonstration three-dimensional calculations for a pancake chamber with off-center valve are also presented.

## IV. Numerics and Modeling

Although in the principle, the pdf/Monte Carlo approach can be used on its own as a solution procedure for multidimensional flows,[20] at present it lacks a robust algorithm for the calculation of the mean pressure field. For this reason a coupling of the Monte Carlo to a finite-volume procedure is adopted. In this section we present in turn the salient features of the finite-volume side, the Monte Carlo side, coupling of the two sides, and specification of initial and boundary conditions.

### Finite Volume Side

Although the flows considered are of nearly uniform density, the solution algorithm is applicable to variable-density flows as well. Thus the principle equations solved are those for the mean momentum, mean pressure, turbulent kinetic energy $K$, the viscous dissipation rate of turbulent kinetic energy $\epsilon$, and mean internal energy; mean density is calculated using an equation of state. We will focus on the modeling of the mean momentum equation; the incompressible form suffices for this discussion. In Cartesian tensor notation this equation is

$$\frac{\partial\langle U_j\rangle}{\partial t}+\langle U_i\rangle\frac{\partial\langle U_j\rangle}{\partial x_i}+\frac{\partial\langle u_i u_j\rangle}{\partial x_i}=-\frac{1}{\rho}\frac{\partial\langle p\rangle}{\partial x_j}+\nu\frac{\partial^2\langle U_j\rangle}{\partial x_i\,\partial x_i} \tag{3}$$

Here $\nu = \mu/\rho$ is the kinematic viscosity, and all mean quantities are interpreted as integrals over the pdf in the sense of Eqs. (1) and (2).

At the level of Eq. (3), it is the treatment of $\langle u_i u_j\rangle$ that distinguishes the various statistical turbulence closures. In the $k$-$\varepsilon$ model, modeled transport equations are solved for the turbulent kinetic energy $k$ ($k \equiv \langle u_i u_i\rangle/2$) and its viscous dissipation rate $\epsilon$. The Reynolds stress term $\langle u_i u_j\rangle$ in Eq. (3) is modeled by drawing an analogy between turbulent transport of momentum and molecular transport: The molecular viscosity $\mu$ is replaced by an effective viscosity $\mu_{\text{eff}} = \mu + \mu_t$, where $\mu_t$ is a turbulent viscosity based on $k$ and $\epsilon$. In the present work standard modeled equations for $k$ and $\epsilon$ and the usual values for all model constants are used.[8,9,29,30]

In Reynolds stress closures the Reynolds stress term in Eq. (3) remains explicitly in evidence, and up to six additional equations governing the evolution of $\langle u_i u_j\rangle$ are added to the set to be solved. At the level of the mean momentum equations, the pdf/Monte Carlo approach is equivalent to a Reynolds stress closure, the difference being that the Reynolds stresses are computed from the pdf [Eq. (2)] rather than from modeled equations for $\langle u_i u_j\rangle$; compared to Reynolds stress models, closure problems associated with convective transport are overcome in the pdf method.

We now turn to the finite-volume solution algorithm. The method used is based on the PISO algorithm developed by Issa.[31] Governing equations are discretized in a curvilinear orthogonal coordinate system using a conservative staggered grid arrangement. The discretized equations are solved implicitly using a predictor/corrector scheme. A combination of standard (first-order) upwind and central differencing has been implemented for the convective terms in the mean momentum equation. Thus, the convective flux of momentum $\mathscr{F}$ for each cell fact is calculated as

$$\mathscr{F} = (1-\gamma)\mathscr{F}_u + \gamma\mathscr{F}_c \tag{4}$$

Here $\gamma$ is a constant specified a priori ($0 \le \gamma \le 1$), and the subscripts $u$ and $c$ refer to upwind and central differencing, respectively. Low values of $\gamma$ generate more stable solutions but may be highly diffusive; higher values of $\gamma$ are generally more accurate but may lead to oscillations. Studies of the effects of grid density and choice of $\gamma$ appear in Sec. V.

### Monte Carlo Side

The Lagrangian algorithm and associated turbulence models are now described. We consider an ensemble of $N$ notional particles. The $n$th particle is characterized by three position coordinates $\underline{x}^{(n)}$, three velocity components $\underline{U}^{(n)}$, $\sigma$ scalars $\underline{\phi}^{(n)}$, a density $\rho^{(n)}$ (from an equation of state), a weight $w^{(n)}$ representing the particle mass, and one or more timing variables $\tau_m^{(n)}$, depending on the number of particle interaction models used (these will be described presently). In a time interval $\delta t$, particle positions, velocities, and scalars evolve according to

$$x_i^{(n)}(t+\delta t) = x_i^{(n)}(t) + U_i^{(n)}\delta t \tag{5}$$

$$U_i^{(n)}(t+\delta t) = U_i^{(n)}(t) - \frac{1}{\rho^{(n)}}\frac{\partial\langle p\rangle}{\partial x_i}\delta t + g_i\delta t + \Delta U_i^{(n)} \qquad (i = 1,2,3) \tag{6}$$

$$\phi_\alpha^{(n)}(t+\delta t) = \phi_\alpha^{(n)}(t) + S_\alpha^{(n)}\delta t + \Delta\phi_\alpha^{(n)} \qquad (\alpha = 1,\dots,\sigma) \tag{7}$$

where $g$ is a body force vector (per unit mass), and $\underline{S}^{(n)}$ is a reaction source term. Here $\Delta U_i^{(n)}$ is the particle velocity increment due to viscosity and the fluctuating pressure gradient, and $\Delta\phi_\alpha^{(n)}$ is the increment in particle scalar composition caused by molecular diffusion. Valid closure models for these increments may include any functional of the pdf plus turbulence scale information (e.g., the turbulence time scale $\tau = k/\epsilon$). It may be seen that convection [Eq. (5)] and the effects of the mean pressure gradient and body forces [Eq. (6)] and chemical reaction [Eq. (7)] are treated without approximation.

It is convenient to introduce two spatial grids in the Monte Carlo calculations: cells and bins. Cells are used for spatially interpolating mean quantities that are needed as coefficients in the modeled particle equations (e.g., $\partial\langle p\rangle/\partial x_i$ and $\tau$); they also define the local spatial regions over which particles can interact in models of the particle interaction kind (see the following). Bins, which may or may not coincide with cells, are used for ensemble averaging over particles to obtain local estimates of mean quantities. Convection in physical space is treated without direct reference to the grids, so that numerical diffusion is avoided.

### *Modeling*

For the velocity increment two classes of models are considered. In the first, $\Delta U_i^{(n)}$ of Eq. (6) is represented by a simplified Langevin equation,[20–23]

$$\Delta U_i^{(n)} = -(\tfrac{1}{2}+\tfrac{3}{4}C_0)(U_i^{(n)} - \langle U_i \rangle)\delta t/\tau + (C_0\epsilon)^{\frac{1}{2}}\delta W_i(t) \quad (8)$$

where $C_0$ is a model constant, $\tau$ is the turbulence time scale, and $\underline{W}(t)$ is an isotropic Wiener process. The latter is a Markovian stochastic process whose increments $\delta\underline{W}(t) = \underline{W}(t+\delta t) - \underline{W}(t)$ have a joint-normal distribution with zero means $(\langle W_i(t)\rangle = 0)$ and an isotropic covariance matrix $[\langle \delta W_i(t)\delta W_j(t)\rangle = \delta_{ij}\delta t$, where $\delta_{ij}$ is the Kronecker delta]. This model results in a return-to-isotropy of the Reynolds stresses and a decay of turbulent kinetic energy. The corresponding Reynolds stress evolution equation is[23]

$$\frac{\partial\langle u_i u_j\rangle}{\partial t} + \langle U_k\rangle\frac{\partial\langle u_i u_j\rangle}{\partial x_k} + \frac{\partial\langle u_i u_j u_k\rangle}{\partial x_k} + \langle u_i u_k\rangle \times\frac{\partial\langle U_j\rangle}{\partial x_k} + \langle u_j u_k\rangle\frac{\partial\langle U_i\rangle}{\partial x_k} = -2C_1\epsilon b_{ij} - \tfrac{2}{3}\epsilon\delta_{ij} \quad (9)$$

Here $b_{ij} = \langle u_i u_j\rangle/2k - \delta_{ij}/3$ is the normalized anisotropy tensor, and $C_1 = (3C_0+2)/2$. Equation (9) corresponds to Rotta's linear return-to-isotropy model for the Reynolds stresses[10,32] plus isotropic dissipation. With $C_0 = 2.1$ (the standard value[22]), the value of the Rotta constant is $C_1 = 4.15$. This is close to the value $C_1 = 4.5$, which is found to yield good results in free shear flows in the absence of an explicit model for the "rapid" pressure terms, that is, terms involving the mean velocity gradients on the right-hand side of Eq. (9).

The second class of models is the particle interaction type.[20,33] Here the improved form of these models developed by Pope[33] is implemented. According to these models, the velocity of a particle changes at discrete times via an interaction with a nearby second particle, the frequency of the interactions being proportional to $\tau^{-1}$. The selection of particles for interaction is biased in favor of those that have not recently undergone an interaction. Thus, it is necessary to track each particle's "age" since last mixing.

With particle interaction models the viscous effect and fluctuating pressure gradient effects are modeled separately. Viscous effects are simulated by a stochastic mixing model, whereas a stochastic reorientation model handles the effects of the fluctuating pressure gradient. On each computational time step, particles selected for mixing are paired at random within cells. A stochastic mixing event proceeds as follows. Two particles $p$ and $q$ selected and paired for mixing have their velocities incremented according to

$$\Delta\underline{U}^{(p)} = \beta[-\underline{U}^{(p)}(t) + \bar{\underline{U}}^{(pq)}], \Delta\underline{U}^{(q)} = \beta[-\underline{U}^{(q)}(t) + \bar{\underline{U}}^{(pq)}] \quad (10)$$

where $\bar{\underline{U}}^{(pq)}$ is the mean of their initial velocities, $\bar{\underline{U}}^{(pq)} = [\underline{U}^{(p)}(t) + \underline{U}^{(q)}(t)]/2$. Here $\beta$ is a random variable $(0 \le \beta \le 1)$ prescribing the degree of mixing. For $\beta = 0$ the velocities of the two particles remain unchanged; for $\beta = 1$ the velocity of each particle after mixing is equal to the mean of their initial velocities. The effect of this model is to leave the mean velocities unchanged while causing the turbulent kinetic energy to decay. The rate of decay is set by a model constant $C_u$ that appears in the age distribution;[33] for consistency with the decay of homogeneous turbulence $(\mathrm{d}k/\mathrm{d}t = -\epsilon)$, $C_u \equiv 1.0$.

Stochastic reorientation, on the other hand, causes the Reynolds stress tensor to approach isotropy while leaving the mean velocities unchanged. Thus, two particles $p$ and $q$ selected and paired for stochastic reorientation have their velocities modified according to

$$\Delta\underline{U}^{(p)} = -\underline{U}^{(p)}(t) + \bar{\underline{U}}^{(pq)} + \tfrac{1}{2}\boldsymbol{\eta}\,\Delta U^{(pq)}$$

$$\Delta\underline{U}^{(q)} = -\underline{U}^{(q)}(t) + \bar{\underline{U}}^{(pq)} - \tfrac{1}{2}\boldsymbol{\eta}\,\Delta U^{(pq)} \quad (11)$$

where $\Delta U^{(pq)}$ is the magnitude of the distance separating particles $p$ and $q$ in velocity space $(\Delta U^{(pq)} = |\underline{U}^{(p)} - \underline{U}^{(q)}|)$, and $\boldsymbol{\eta}$ is a randomly oriented unit vector. A model constant $C_r$ appears in the specification of the age distribution for the stochastic reorientation model. The Reynolds stress evolution from the combination of these two particle interaction models follows Eq. (9), with $C_1 = C_r$; we take $C_r = 4.5$.[23] Thus, in homogeneous turbulence $(\langle u_i u_j u_k\rangle = 0)$, the combination of these two particle interaction models yields (for equivalent values of model constants) the same evolution of the Reynolds stresses as the simplified Langevin model. For inhomogeneous turbulence, different velocity pdf values from the two classes of model (e.g., different values of $\langle u_i u_j u_k\rangle$) lead to different Reynolds stress evolutions.

### *Numerical Algorithm*

Formally, the process of extracting mean quantities from the pdf consists of evaluating moments of the pdf in the appropriate sample space [Eqs. (1) and (2)]. In the Monte Carlo method mean quantities are estimated by ensemble averaging over the particles within bins. The mass- or Favre-averaged mean of any function of the velocities and scalars at position $\underline{x}_m$ and time $t$ can be estimated as the weighted ensemble average over the $N_m$ particles in the $m$th bin at position $\underline{x}_m$ at time $t$. For example, an estimate of the Favre-averaged Reynolds stresses at $\underline{x}_m$ is

$$\widetilde{u_i'' u_j''} \approx \overline{(u_i'' u_j'')}_{N_m} \equiv \frac{1}{N_m}\sum_n w^{(n)}[U_i^{(n)} - \overline{(U_i)}_{N_m}] \times[U_j^{(n)} - \overline{(U_j)}_{N_m}]/\frac{1}{N_m}\sum_n w^{(n)} \quad (12)$$

where

$$\tilde{U}_i \approx \overline{(U_i)}_{N_m} \equiv \frac{1}{N_m}\sum_n w^{(n)}U_i^{(n)}/\frac{1}{N_m}\sum_n w^{(n)} \quad (13)$$

The statistical error in this estimate is of order $N_m^{-1/2}$. These bin averages are smoothed spatially using tensor product three-dimensional cross-validated cubic smoothing splines[34,35] to obtain smooth profiles of mean quantities and to reduce statistical error. The statistical error in the splined profiles is of order $N^{-1/2}$.

Two forms of particle distribution control are exercised in the course of the calculations. Particle positions in physical space are shifted on each time step to ensure that, at the resolution of cells, the particle volume is consistent with the fluid volume. This mean continuity requirement nominally is satisfied automatically in the course of the calculations,[20] but statistical and discretization errors lead to small deviations.

A second set of corrections maintains the particle number density in physical space and the distribution of particle weights so that statistical error is uniformly distributed. It may be seen from Eqs. (12) and (13) that particle weights can be modified in many ways that leave weighted averages unaltered. For example, the weights of all particles can be multiplied by any constant. Particles can be "cloned"; i.e., a particle of weight $w$ can be split into two particles of weight $w/2$ with the same properties at the same physical location, and particles of weight $w$, less than some preferred weight $\hat{w}$, can be "annihilated" or removed with probability $1 - w/\hat{w}$ and "promoted" from weight $w$ to weight $\hat{w}$ with probability $w/\hat{w}$ with only a small statistical error. These ideas are used to keep particle weights nearly uniform within cells, keep the particle number density nearly uniform in physical space, ensure that only particles of equal weights can pair in particle interaction models, and keep the total number of particles $N$ under control when there is a net inflow or outflow of fluid from the computational domain.

In the axisymmetric calculations additional operations are required. Particles are confined to the radial-axial ($r$-$z$) plane and their weights and velocity components modified via a procedure that retains the three-dimensional nature of the fluctuating velocity field while taking advantage of the fact that mean quantities are independent of azimuth angle.[20,21] Particle weights $w^{(n)}$ are proportional to the particle's radial coordinate; that is, particles at large radial distances from the axis of symmetry represent larger volumes of fluid than particles near the axis. The system of variable particle weights is also used to account for nonuniform fluid density in variable-density flows.

The Monte Carlo method described earlier provides an exact solution to a modeled pdf transport equation in the limit as the number of particles $N$ approaches infinity and the numerical time step $\delta t$ approaches zero.[20,21] For a finite number of particles the statistical error is of order $N^{-1/2}$. Typically, on the order of $10^4$ particles have proven to be adequate for statistically one-dimensional flows; here $10^5$ to $10^6$ have been used for statistically two- and three-dimensional flows. Explicit time differencing is used in the Monte Carlo calculations with the time step $\Delta t$ taken to be a fraction of the turbulence time scale $\tau$.

### Coupling

At the completion of a finite-volume time step, mean velocities, mean pressure gradients, and the turbulence time scale are passed from the finite volume to the Monte Carlo side of the code. The Monte Carlo side is then advanced one time step as outlined earlier; the resulting Reynolds stress values are fed back to the mean momentum equation on the finite-volume side for the beginning of the next step. On each time step particle velocities on the Monte Carlo side are corrected to finite-volume mean velocities at the resolution of cells. In variable-density flows the mean density as well as the mean velocity must be kept consistent on the two sides of the calculation.

### Initial and Boundary Conditions

Initial conditions for the axisymmetric calculations are generally the same as those used by El Tahry[9] in his study of the axisymmetric annular port flow. The calculations are started at top dead center with a quiescent mean velocity field, with turbulent kinetic energy and its dissipation rate scaled to the mean piston speed $\bar{V}_p$, and with the isotropic Reynolds stresses having a joint-normal distribution,

$$\langle \underline{U} \rangle_0 = 0, \qquad k_0 = 0.09\bar{V}_p^2, \qquad \langle u_i u_j \rangle_0 = 2k_0\delta_{ij}/3$$

$$\epsilon_0 = 0.4k^{2/3}/y \tag{14}$$

where $y$ is the distance to the nearest solid boundary, and subscript 0 refers to time $t = 0$.

Boundary conditions are specified as follows. For solid walls mean velocities are set to the boundary velocity $\underline{U}_b$. Adopting the usual approach taken in $k$-$\epsilon$ modeling studies,[9,29,30] we use the log law applicable to one-dimensional steady turbulent boundary layers to set the level of the wall shear stress in the mean momentum equation. No information from the wall is needed for the $k$ equation, since the flux of $k$ is zero at the wall. The dissipation rate in the cell adjacent to the wall $\epsilon_{nw}$ is prescribed via the standard wall expression.[8,9] Thus, the boundary conditions can be expressed as

$$\langle \underline{U} \rangle_w = \underline{U}_b, \qquad \epsilon_{nw} = C_\mu^{3/4} k^{3/2}/\kappa\, \Delta y \tag{15}$$

where the subscript $w$ denotes a value at the wall, $\Delta y$ is the normal distance from the wall to the cell center adjacent to the wall, and $C_\mu$ and $\kappa$ are standard model constants in the $k$-$\epsilon$ model.[8,9] On the Monte Carlo side specular reflection boundary conditions are specified for particle velocities; this is consistent with zero turbulent flux boundary conditions.

The finite-volume calculation is performed for a single-cell width pie-shaped wedge in three dimensions. The two azimuthal faces are tied together, thus enforcing axisymmetry. On the axis of symmetry the element faces degenerate to zero area, thus ensuring zero flux at the pole.

At inflow boundaries, the mass flux entering the cylinder is calculated from the pressure drop across the entrance and an orifice model.[29] Profiles of mean velocity are taken to be uniform for the annular port and a 1/8-power law profile for the central port. For turbulence quantities uniform profiles of $k$ and $\epsilon$ are specified[9]:

$$k_{\text{in}} = 0.01\, W_{\max}^2, \qquad \epsilon_{\text{in}} = 0.50k^{3/2}/\Delta R \tag{16}$$

where $W_{\max}$ is the peak mean axial velocity at the inlet, and $\Delta R$ is the annulus width for the annular port case ($\Delta R = 4$ mm) or the inlet pipe radius for the central port case ($\Delta R = 9.375$ mm). The radial, aximuthal, and axial components of the Reynolds stress at the inlet are given by $\langle u_r^2 \rangle = 0.5k$, $\langle u_\theta^2 \rangle = 0.7k$, $\langle u_z^2 \rangle = 0.8k$, respectively, and the only nonzero component of the shear stress is $\langle u_r u_z \rangle = 0.2k$.[9] The pdf of entering velocity is joint normal.

## V. Results

We concentrate on results for the central port; further results for the annular port including passive scalar statistics may be found in Ref. 27. Demonstration calculations for a three-dimensional configuration are presented. Before the results are shown the baseline numerical parameters are specified.

### Baseline Numerical Values

In axisymmetric cases the finite-volume grid is uniform in $z$ (expanding/contracting with the piston motion) and piecewise uniform in $r$ to accommodate a finer mesh spacing under the port. Grids used are summarized in Table 1: The 62 × 62 meshes have been selected as our baseline with $\gamma = 0$ for maximum stability. The computational time step expressed in crank angle degrees $\Delta\theta$ is also given in Table 1. The explicit implementation of the Reynolds stress terms and the use of values of $\gamma$ different than zero [Eq. (4)] can lead to oscillations for large $\Delta\theta$. Typically we find that, once $\Delta\theta$ is small enough that oscillations are suppressed, further reduction yields little change in calculated mean and rms velocities. Results on the 62 × 62 mesh are not entirely grid-independent (as will be shown below) but suffice for this assessment of the new method.

Table 1 Finite-volume meshes for axisymmetric flows[a]

| Designation | Flow type | $n_r$ | $n_z$ | $\Delta\theta$ |
|---|---|---|---|---|
| C1 | Central port | 43 | 43 | 0.40 |
| C2 | Central port | 62 | 62 | 0.20 |
| C3 | Central port | 88 | 88 | 0.10 |
| A0 | Annular port | 28 | 28 | 1.0 |
| A1 | Annular port | 43 | 43 | 0.50 |
| A2 | Annular port | 62 | 62 | 0.25 |
| A3 | Annular port | 88 | 88 | 0.125 |
| A4 | Annular port | 126 | 126 | 0.0625 |

[a] There are $n_r$ cells in the radial ($r$) direction, $n_z$ cells in the axial ($z$) direction, and the computational time step in crank angle degrees is $\Delta\theta$.

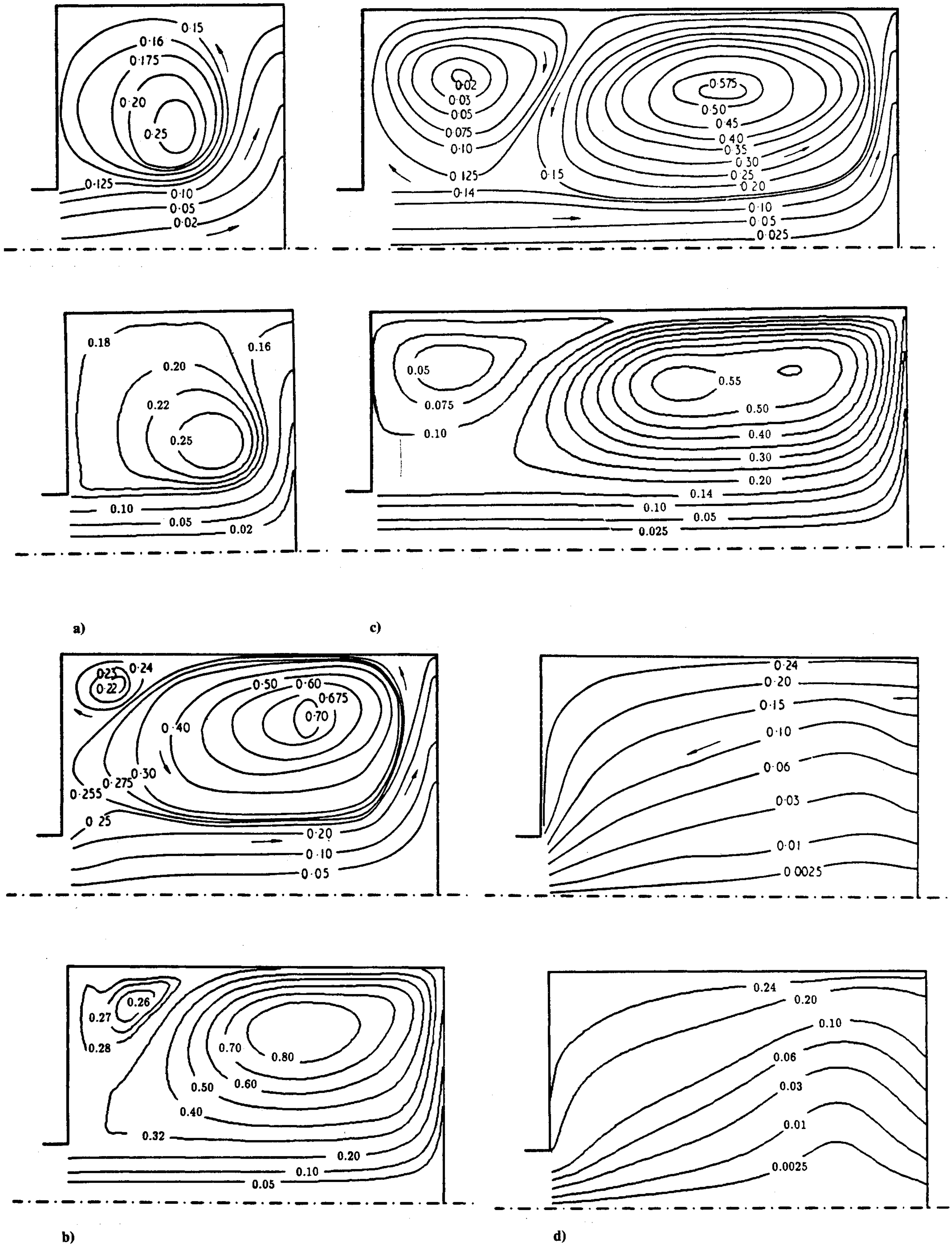

**Fig. 2 Contours of the normalized mean stream function for the central port. Top figure of each pair shows measurements[28]; bottom figure shows calculations. Calculations at 36 and 90 deg are from coupled Monte Carlo finite-volume runs; those at 144 and 270 deg are from $k$-$\epsilon$/finite volume: a) 36 deg; b) 90 deg; c) 144 deg; d) 270 deg.**

We concentrate on results for the first two crank angles, 36 and 90 deg. Unless otherwise specified, 21 × 21 spline basis functions in the $r$-$z$ plane and nominally 250,000 computational particles are used in the Monte Carlo calculations (the number of particles varies in the course of the calculations, as explained in Sec. IV). Monte Carlo cells coincide with bins, and the number of Monte Carlo cells is equal to the number of finite-volume cells.

### Central Port

For this flow, particle interaction models for particle velocities have been used. Calculated (mesh C2, $\gamma = 0$) and measured[28] streamlines are shown in Fig. 2. At early crank angles (Fig. 2a), the flow consists of a jet from the entrance to the piston and a single large toroidal vortex. By 90 deg (Fig. 2b), a small secondary recirculation zone has developed in the head-cylinder wall corner; this structure grows to occupy about one-third of the chamber length at 144 deg (Fig. 2c). Then, at 270 deg (Fig. 2d), all evidence of vortical flow structure has disappeared and we are left with a simple sink flow. Calculated stream functions on the C2 grid qualitatively duplicate the measured flow patterns; quantitative agreement is reasonable good. It should be noted that there are large errors associated with extracting numerical values of stream function from the measured velocity fields.[28] Statistical error in the splines causes the calculated value of the stream function at the cylinder wall to differ from the experimental value. Although it may not be evident in Fig. 2, the splined mean velocity does (by construction) satisfy the boundary condition that the mean velocity is equal to the piston velocity at the piston face.

In Figs. 3 and 4 calculated profiles of mean and rms axial velocity are compared with measurements. Here and in the following, the axial rms velocity from $k$-$\epsilon$ calculations is deduced assuming isotropy of the normal stresses: $\langle u_z^2 \rangle = 2k/3$. For the mean velocities (Fig. 3) agreement with measurement is very good. It may be seen that differences between mean velocity profiles obtained from the coupled calculations vs those from $k$-$\epsilon$/finite volume alone are small.

Calculated rms turbulence levels (Fig. 4) are quite low at the first crank angle (36 deg). At 90 deg, the general profile shapes are well matched, but both models tend to overshoot the peak in the high shear region of the jet, and both sets of calculations are high on the centerline as well. Thus, the model matches experimental mean velocity profiles at both crank angles, yet underpredicts the rms velocity severely at the earlier time and overpredicts it at the later time. This leads us to suspect the measured turbulence levels at 36 deg, $z = 10$ mm. These levels are unusually high: The peak rms velocity is over 50% of the centerline mean jet velocity. At 90 deg, mean velocities are higher, yet turbulence levels are lower than those at 36 deg. A second possible explanation for the discrepancy between model and measurement is the inflow boundary conditions: The time-dependent inlet mean velocity profiles specified in Ref. 29 yield better agreement between calculated and measured rms velocities at 36 deg than that found here.

The similar behavior of the two models is to be expected for this flow: It is a flow of nearly uniform density and is dominated by the strong incoming jet. The simple nature of the pdf turbulence models (i.e., no rapid pressure term) and the use of the standard dissipation equation for the turbulence time scale $\tau$ also contribute to the relatively small differences observed between the two computational approaches.

Much of the difference that is observed between Monte Carlo and $k$-$\epsilon$ rms velocities can be attributed to anisotropy in the normal components of the Reynolds stresses in the Monte Carlo calculations. In the highest shear regions of the flow the axial component tends to be larger than the radial or azimuthal components; in low shear regions the axial component tends to be the smallest of the three. Thus, the turbulent kinetic energy $k = (\langle u_r^2 \rangle + \langle u_\theta^2 \rangle + \langle u_z^2 \rangle)/2$ from the pdf model is not as different from the $k$-$\epsilon$ results as Fig. 4 implies.

Results are relatively insensitive to the choice of $\gamma$; for this flow the strong incoming jet is aligned with the computational grid so that numerical diffusion may be minimal in the regions where the steepest velocity gradients occur. Mesh density has a strong influence, however. Reducing the number of cells

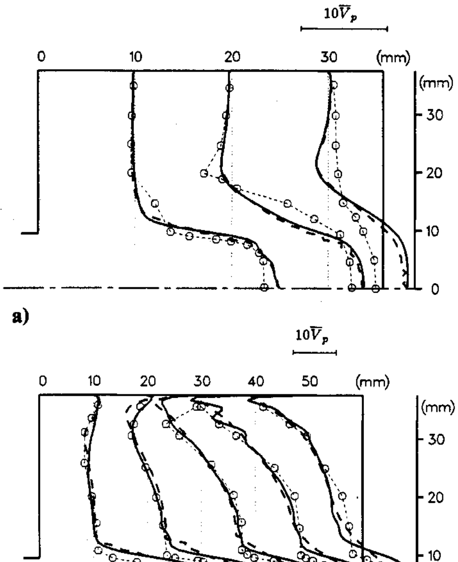

Fig. 3 Radial profiles of mean axial velocity $\langle U_z \rangle$ at several axial stations for the central port, normalized by the piston speed $\bar{V}_p$. Solid lines are coupled Monte Carlo finite-volume calculations; bold dashed lines are $k$-$\epsilon$/finite-volume calculations; symbols and light dashed lines are experimental data[28]: a) 36 deg; b) 90 deg.

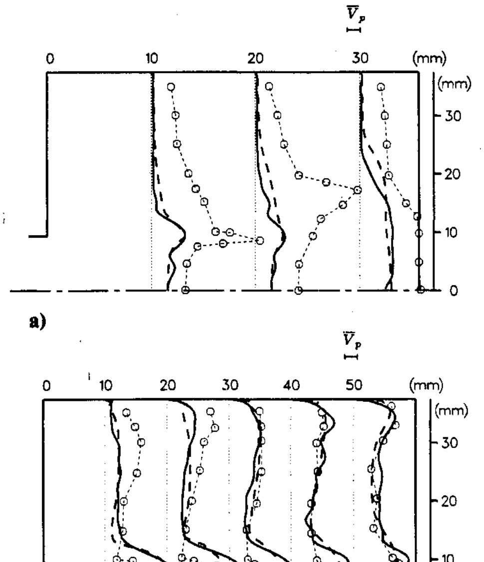

Fig. 4 Radial profiles of rms axial velocity $\langle u_z^2 \rangle^{1/2}$ at several axial stations for the central port, normalized by the mean piston speed $\bar{V}_p$: a) 36 deg; b) 90 deg. Symbols as in Fig. 3.

from 62 × 62 (C2) to 43 × 43 (C1) dramatically alters the flow pattern; the small secondary vortex visible in the measurements at 90 deg (Fig. 2b) is not present in the coarser mesh calculation. This is probably a result of the wall boundary condition [Eq. (15)]: The value of the length scale $l = k^{3/2}/\epsilon$ close to the wall is sensitive to the width of the computational cell adjacent to the wall. Mean and rms velocity profiles on the three meshes $C1 \rightarrow C3$ of Table 1 vary significantly from C1 to C2, but show little further change in going to finer meshes.

### Annular Port

Results for the annular port appear in Figs. 5–8. Here the simplified Langevin equation [Eq. (8)] has been used for particle velocities.

Streamlines at 90 deg show the salient features of the flow pattern (Fig. 5). Separation at the annulus edge leads to a double counter-rotating vortex pattern, and a third recirculation zone develops along the cylinder wall close to the piston. As in the central port case, the flow degenerates to a simple sink flow by 270 deg on the exhaust stroke (not shown). Quantitative agreement between calculated and measured stream function values is generally good at all crank angles.[27]

Comparison of mean (Fig. 6) axial velocities for the baseline mesh (A2) reveals levels of agreement that are, as a whole, not as satisfactory as for the central port case. The most notable discrepancy is the severe undershooting of the mean and rms velocities at 36 deg, $z = 20$ mm. The peak jet velocity is also underpredicted at the measurement station closest to the head ($z = 10$ mm) for 36, 90, and 144 deg. At 90 deg, the calculated jet tends to lie further from the cylinder wall than the data show (Fig. 6b).

Calculated turbulence levels also exhibit behavior that differs from measurements in some respects (Fig. 7). Close to the head at both 36 and 90 deg, calculations show a double-peaked profile of rms axial velocity that is not present in the experimental data. It seems reasonable to expect two peaks in turbulence intensity, one in each of the steep mean velocity gradient zones on each side of the incoming jet. These double peaks are present in the 90 and 144 deg measurements at $z = 20$ and 30 mm, respectively.

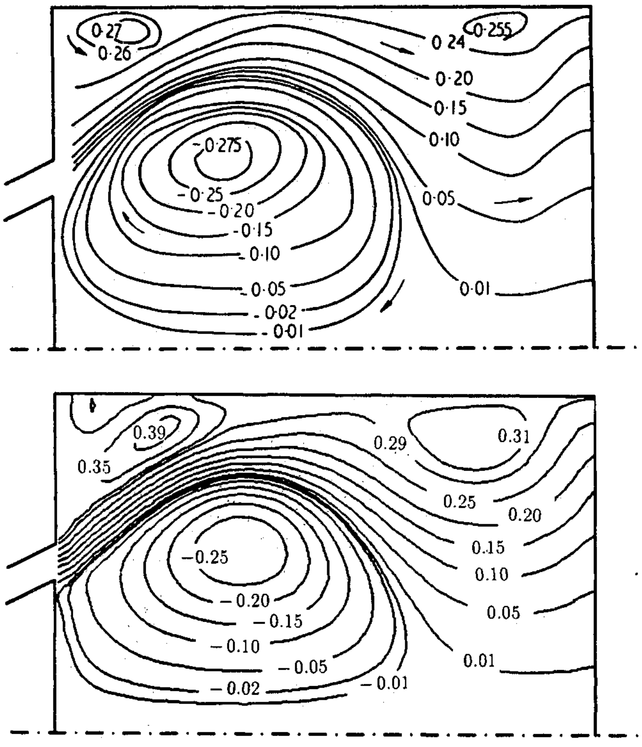

Fig. 5 Contours of the normalized mean stream function for the annular port at 90 deg after top dead center. Top figure shows measurements[28]; bottom figure shows calculations.

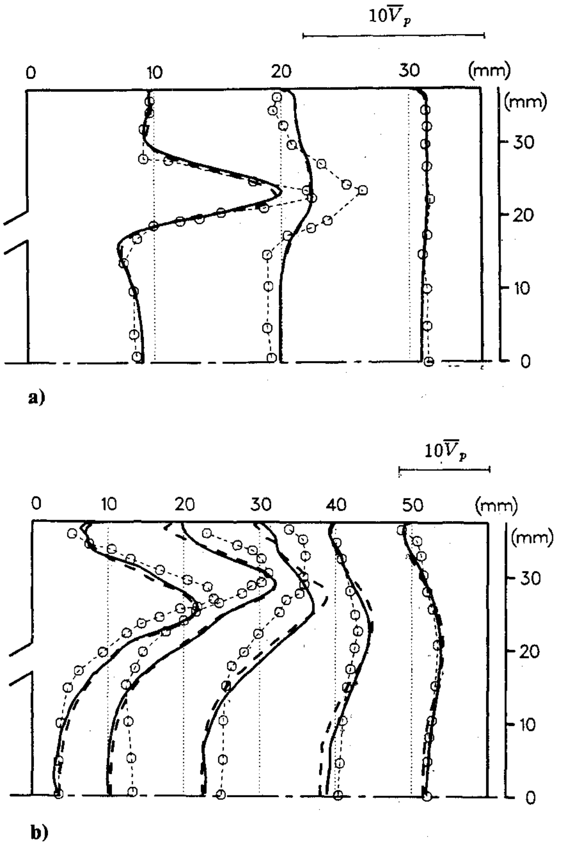

Fig. 6 Radial profiles of mean axial velocity $\langle U_z \rangle$ at several axial stations for the annular port, normalized by the mean piston speed $\bar{V}_p$: a) 36 deg; b) 90 deg. Symbols as in Fig. 3.

Differences between Monte Carlo finite-volume mean velocity profiles and those obtained using the finite-volume algorithm alone are again minimal (Fig. 6). More differences may be seen in the rms axial velocity profiles (Fig. 7); here the coupled calculation tends to yield higher turbulence levels in the strong shear regions of the jet and lower levels near the centerline, in better agreement with measurements than the finite-volume results. As was pointed out for the central port case, this can be attributed mainly to anisotropy of the Reynolds stresses.

This flow is computationally more difficult than the central port configuration for two reasons: 1) it may be expected that, because of the orientation of the inlet jet at 30 deg to the grid, this flow would be particularly susceptible to numerical diffusion; and 2) the incoming jet impinges directly on the cylinder wall so that wall boundary conditions may be playing a stronger role here. The relatively small differences noted between pdf and $k$-$\epsilon$ results can, as before, be atributed to the nature of the flowfield and the models used.

Figure 8 illustrates the effect of variations in mesh density and differencing scheme. The peak mean velocity at $z = 10$ mm, $\theta = 36$ deg is shown as a function of mesh spacing $n_r^{-1}$ and of $\gamma$. For any value of $\gamma$ less than unity, convective differencing is first-order accurate. Thus, we expect that for sufficiently small mesh spacings the velocity at a point should approach its asymptotic ($n_r^{-1} \rightarrow 0$) value linearly with $n_r^{-1}$. The curves of Fig. 8 appear to become linear for small $n_r^{-1}$, except for a small deviation in the $\gamma = 0.7$ curve for small $n_r^{-1}$. Although it is not conclusive that the four curves for different $\gamma$ are converging to the same value, it is clear that the separation among the curves is decreasing as $n_r^{-1}$ decreases.

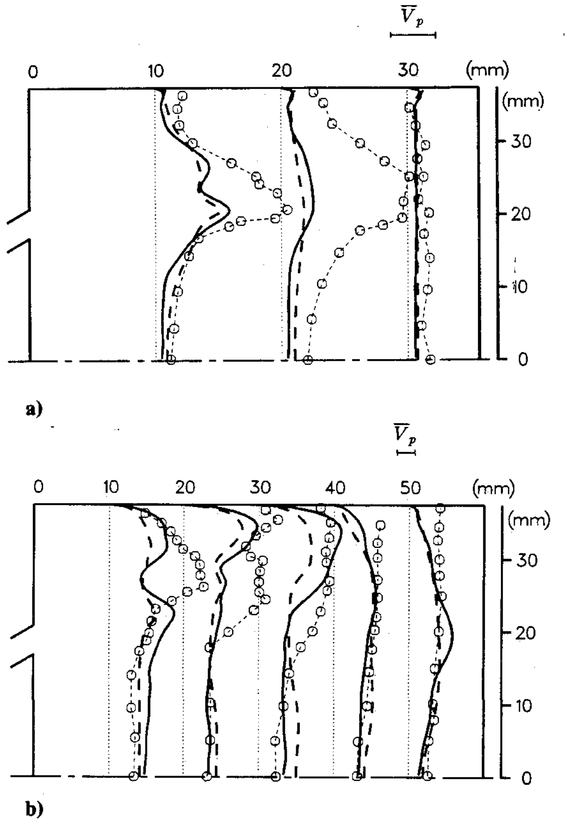

**Fig. 7 Radial profiles of rms axial velocity $\langle u_z^2 \rangle^{1/2}$ at several axial stations for the annular port, normalized by the mean piston speed $\bar{V}_p$: a) 36 deg; b) 90 deg. Symbols as in Fig. 3.**

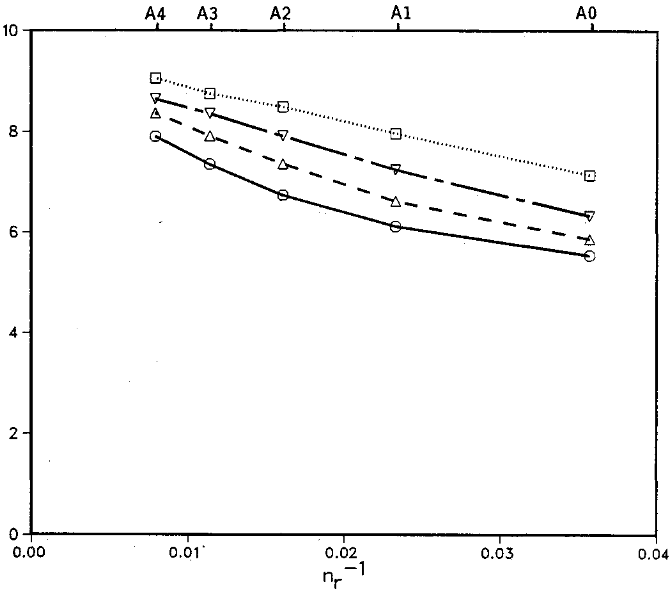

**Fig. 8 Normalized peak mean axial velocity vs mesh density $n_r^{-1}$ for the annular port at 36 deg after top dead center, $z = 10$ mm: ——, $\gamma = 0.0$; - - - - - -, $\gamma = 0.3$; — — — $\gamma = 0.5$; · · · · · ·, $\gamma = 0.7$.**

Two points are made concerning these results. First, convergence is slow and (for coarse meshes) nonlinear. Thus, the modest gain in going from A0 ($28^2$) to A1 ($43^2$) for $\gamma = 0.0$ might be improperly interpreted as grid independence, although, in fact, we are 10–15% below the apparent converged value even on the A4 ($126^2$) mesh. Trends for other point quantities are similar. Second, mesh refinement tests of this kind are complicated by nonlinear coupling among equations and by the effect of mesh spacing on boundary conditions. Typically $20^3$ to $30^3$ cells have been used in three-dimensional engine simulations.[1-7]

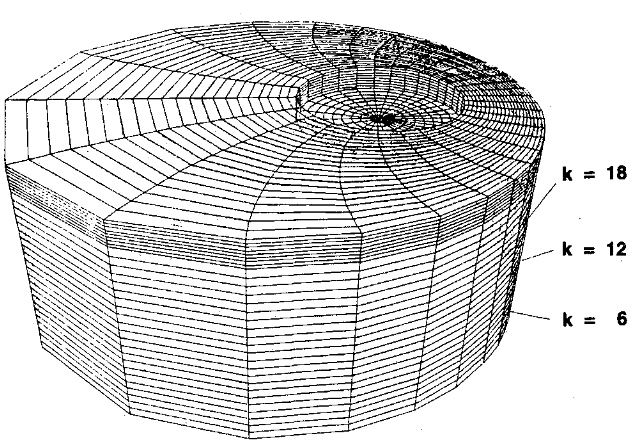

**Fig. 9 Computational mesh for three-dimensional pancake chamber calculations with an off-center valve. Labels refer to three planes stacked normal to the cylinder axis.**

The influence of numerical parameters on the Monte Carlo side of the calculation has also been examined. The number of computational particles has been varied by a factor of two about the baseline value (125,000–500,000 particles) without significantly affecting calculated mean velocity or turbulence levels. The splined profiles tend to be smoother when more particles are used. For the axisymmetric flows we find that a minimum of 17 × 17 basis functions are required to adequately resolve the spatial variations in mean velocity and Reynolds stresses; use of a smaller number clips the peaks. As long as the number of basis functions is sufficient to resolve the profiles of interest, further increases should not alter the results significantly, since cross validation is being used.[34,35] Systematic studies of statistical error for the Monte Carlo algorithm in one spatial dimension may be found in Ref. 21; errors introduced by splining are analyzed in Refs. 34 and 35.

El Tahry[9] noted larger improvements in both mean and rms velocities in going from a $k$-$\epsilon$ model to a Reynolds stress model than has been observed here in going from $k$-$\epsilon$ to a pdf approach. In particular, he noted a dramatic improvement in the mean and rms velocities at 36 deg, $z = 20$ mm. Major differences between the approach used by El Tahry[9] and that used here include the following: 1) an explicit model for rapid pressure terms was included in the Reynolds stress closure used by El Tahry; 2) a different boundary condition for the shear stress (zero flux vs log law) was used in the earlier work; and 3) a more accurate differencing scheme (skew-upwind differencing) was used for the convective terms in the mean momentum equations in Ref. 9.

## Three-Dimensional Results

Three-dimensional runs have been made for a pancake cylinder with off-center valve; an outline of the finite-volume mesh is shown in Fig. 9. The flowfield near the time of ignition is of primary interest in engine applications; hence, the pdf/Monte Carlo algorithm is started following intake valve closure at 252 deg after top dead center with initial conditions taken from the $k$-$\epsilon$ calculations. Compared to the axisymmetric intake flows given earlier, all six Reynolds stress components are now nonzero and the fluid density varies in time.

Contours of turbulent kinetic energy on three planes stacked normal to the cylinder axis at 370 deg (10 deg past top dead center of compression) are given in Fig. 10. It can be seen that the maximum turbulence levels are near the center of the cylinder. The effect of statistical error is evident in these

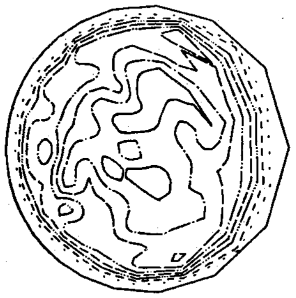

k = 6

········ 2.47 m$^2$/s$^2$

———— 8.98 m$^2$/s$^2$

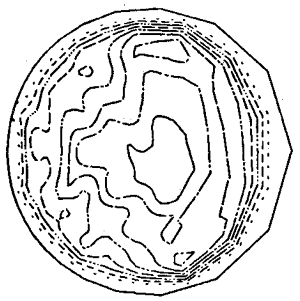

k = 12

········ 3.01 m$^2$/s$^2$

———— 10.43 m$^2$/s$^2$

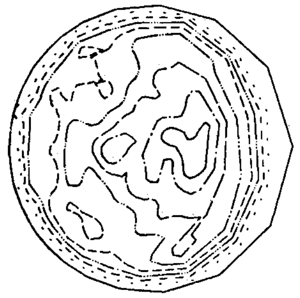

k = 18

········ 2.69 m$^2$/s$^2$

———— 10.74 m$^2$/s$^2$

**Fig. 10 Turbulent kinetic energy contours on three planes labeled in Fig. 9 at 370 deg after top dead center. Contour levels are equally spaced between the given minimum and maximum values.**

profiles: The flow is not perfectly symmetric about a plane containing the cylinder and valve axes. Statistical error can be reduced by increasing the number of computational particles, developing improved smoothing algorithms, or improving the implementation of the stochastic models (variance-reduction techniques of Monte Carlo methods[36]). Smoothing is essential to the successful implementation of these methods in multidimensional flows so that the number of computational particles remains reasonable. Further three-dimensional results including comparisons with measurements will be the subject of future papers. A discussion of aspects of the Monte Carlo algorithm peculiar to three-dimensional applications may be found in Ref. 35.

## VI. Conclusions

These results demonstrate the feasibility of applying the pdf/Monte Carlo method to complex multidimensional transient recirculating turbulent flows. The steep velocity gradients and (in the case of the annular port) inflow inclination to the computational grid provide severe tests of the method.

We conclude that the $k$-$\epsilon$ model and finite-volume solution algorithm yield generally adequate mean and rms velocities for the intake flows provided that solutions are reasonably independent of numerical parameters. The implication for simulations of turbulent reacting in-cylinder flows is that relatively simple models may be adequate to calculate the flowfield prior to intake valve closure and combustion. Details of the turbulence model are expected to be more significant following intake valve closure, when the flow is dominated by the relaxation and redistribution of energy rather than by shear-generated turbulence production. It might be most appropriate to use the Monte Carlo only during the compression and reaction phase of the cycle where the benefits of the pdf approach in dealing with variable-density reacting flows are most significant; this approach has been taken for the preliminary three-dimensional calculations. Anisotropy of Reynolds stresses plays a more important role in flows with swirl and scalar transport; passive scalar computations for the axisymmetric annular port configuration have been reported in Ref. 27.

The pdf modeling approach yields results that are close to those obtained using a $k$-$\epsilon$ model for three reasons. First is the uniform-density shear-driven nature of the test flows. Second, the turbulence time scale is being taken from a conventional modeled dissipation equation; particle-dependent dissipation models are being developed as an alternative.[37] And third, neither the simplified Langevin equation nor the particle interaction models contain terms analogous to the rapid pressure term of second-order closures; generalized versions of the Langevin equation include rapid-pressure effects.[38]

Grid refinement tests reveal that finite-volume numerical errors may be significant for mesh densities typically used in multidimensional engine simulations, particularly for low-order spatial differencing schemes. This may also be limiting the performance of the pdf modeling in the present calculations.

Future work includes quantitative studies of scalar transport (i.e., in-cylinder charge distribution) and flows with swirl. The real potential of the pdf method lies in the calculation of variable-density chemically reacting flows where phenomena such as countergradient diffusion and large density fluctuations should prove more amenable to treatment than in conventional closure models used in multidimensional engine simulations. The present work should be regarded as an intermediate step in applying these methods to transient multidimensional turbulent reacting flows.

## Acknowledgment

The authors thank Stephen B. Pope of Cornell University and M. S. Anand of Allison Gas Turbine Division for several helpful discussions in the course of this work.

## References

[1]Ahmadi-Befrui, B., Brandstätter, W., Kratochwill, H., and Troger, C., "The Influence of Inlet Port Design on the In-Cylinder Charge Mixing," Society of Automotive Engineers Paper 890842, 1989.

[2]Henriot, S., Le Coz, J. F., and Pinchon, P., "Three-Dimensional Modelling of Flow and Turbulence in a Four-Valve Spark Ignition Engine—Comparison with LDV Measurements," Society of Automotive Engineers Paper 890843, 1989.

[3]Diwakar, R., "Assessment of the Ability of a Multidimensional Computer Code to Model Combustion in a Homogeneous-Charge Engine," *SAE Transactions*, Vol. 93, 1984, pp. 85–108.

[4]Kuo, T.-W., and Reitz, R. D., "Computation of Premixed-Charge Combustion in Pancake and Pent-Roof Engines," Society of Automotive Engineers Paper 890670, 1989.

[5]O'Rourke, P. J., and Amsden, A. A., "Three-Dimensional Numerical Simulations of the UPS-292 Stratified Charge Engine," Society of Automotive Engineers Paper 870597, 1987.

[6]Grasso, F., Wey, M.-J., Bracco, F. V., and Abraham, J., "Three-Dimensional Computations of Flows in a Stratified-Charge Rotary Engine," Society of Automotive Engineers Paper 870409, 1987.

[7]Takenaka, Y., Aoyagi, Y., Tsuji, Y., and Joko, I., "3D Numerical Simulation of Fuel Injection and Combustion Phenomena in DI Diesel Engines," Society of Automotive Engineers Paper 890668, 1989.

[8]El Tahry, S. H., "The $k$-$\epsilon$ Equations in Compressible Flows," *Journal of Energy*, Vol. 7, No. 4, 1983, pp. 345–353.

[9]El Tahry, S. H., "A Comparison of Three Turbulence Models in Engine-Like Geometries," *Proceedings of the International Symposium on Diagnostics and Modeling of Combustion in Reciprocating Engines*, Japanese Society of Mechanical Engineering, Tokyo, 1985, pp. 203–213.

[10]Launder, B. E., Reece, G. J., and Rodi, W., "Progress in the Development of a Reynolds Stress Turbulent Closure," *Journal of Fluid Mechanics*, Vol. 68, 1975, pp. 537–566.

[11]Ramos, J. I., Sirignano, W. A., "Turbulent Flow Field in Homogeneous-Charge Spark-Ignition Engines," *Eighteenth Symposium (International) on Combustion*, The Combustion Institute, Pittsburgh, 1981, pp. 1825–1835.

[12]Magnussen, B. F., and Hjertager, B. H., "On Mathematical Modeling of Turbulent Combustion with Special Emphasis on Soot Formation and Combustion," *Sixteenth Symposium (International) on Combustion*, The Combustion Institute, Pittsburgh, 1977, pp. 719–729.

[13]Abraham, J., Bracco, F. V., and Reitz, R. D., "Comparisons of Computed and Measured Premixed Charge Engine Combustion," *Combustion and Flame*, Vol. 60, 1985, pp. 309–322.

[14]El Tahry, S. H., "A Turbulence Combustion Model for Premixed Charge Engines," *Combustion and Flame*, Vol. 79, 1990, pp. 122–140.

[15]Brandstätter, W., and Johns, R. J. R., "The Application of a Probability Method to Engine Combustion and Modeling," *Proceedings of the Institute of Mechanical Engineering*, Vol. C58/83, 1983, pp. 113–124.

[16]Borghi, R., Argeuyrolles, B., Gauffie, S., and Souhaite, P., "Application of a 'Presumed pdf' Model of Turbulent Combustion to Reciprocating Engines," *Twenty-First Symposium (International) on Combustion*, The Combustion Institute, Pittsburgh, 1986, pp. 1591–1599.

[17]Naji, H., Said, R., and Borghi, R. P., "Towards a General Turbulent Combustion Model for Spark Ignition Engines," Society of Automotive Engineers Paper 890672, 1989.

[18]Pope, S. B., "Turbulent Premixed Flames," *Annual Review of Fluid Mechanics*, Vol. 19, 1987, pp. 237–270.

[19]Lundgren, T. S., "Model Equation for Nonhomogeneous Turbulence," *Physics of Fluids*, Vol. 12, No. 3, 1969, pp. 485–497.

[20]Pope, S. B., "Pdf Methods for Turbulent Reactive Flows," *Progress in Energy and Combustion Science*, Vol. 11, 1985, pp. 119–192.

[21]Haworth, D. C., and Pope, S. B., "Monte Carlo Solutions of a Joint pdf Equation for Turbulent Flows in General Orthogonal Coordinates," *Journal of Computational Physics*, Vol. 72, No. 2, 1987, pp. 311–346.

[22]Anand, M. S., and Pope, S. B., "Diffusion Behind a Line Source in Grid Turbulence," *Turbulent Shear Flows*, Vol. 4, edited by L. J. S. Bradbury, F. Durst, B. E. Launder, F. W. Schmidt, and J. H. Whitelaw, Springer-Verlag, Berlin, 1985, pp. 46–61.

[23]Haworth, D. C., and Pope, S. B., "A pdf Modeling Study of Self-Similar Turbulent Free Shear Flows," *Physics of Fluids*, Vol. 30, No. 4, 1987, pp. 1026–1044.

[24]Anand M. S., and Pope, S. B., "Calculations of Premixed Turbulent Flames by pdf Methods," *Combustion and Flame*, Vol. 67, 1987, pp. 127–142.

[25]Haworth, D. C., Drake, M. C., and Blint, R. J., "Stretched Laminar Flamelet Modeling of a Turbulent Jet Diffusion Flame," *Combustion Science and Technology*, Vol. 60, 1988, pp. 287–318.

[26]Anand M. S., Pope, S. B., and Mongia, H. C., "A pdf Method for Turbulent Recirculating Flows," *Turbulent Reactive Flows, Lecture Notes in Engineering*, Vol. 40, Springer-Verlag, Berlin, 1989, pp. 672–693.

[27]Haworth, D. C., and El Tahry, S. H., "Application of a pdf Method to In-Cylinder Flow in Reciprocating Engines," *Proceedings, Seventh Symposium on Turbulent Shear Flow*, Stanford Univ., Stanford, CA, 1989, pp. 13.1.1–13.1.6.

[28]Morse, A. P., Whitelaw, J. H., and Yianneskis, M., "The Flow Characteristics of a Piston-Cylinder Assembly with an Off Center, Open Port," *Proceedings, Institute of Mechanical Energy*, Vol. 194, 1980, pp. 291–299.

[29]Gosman, A. D., Johns, R. J. R., and Watkins, A. P., "Development of Prediction Methods for In-Cylinder Processes in Reciprocating Engines," *Combustion Modeling in Reciprocating Engines*, edited by J. N. Mattavi and C. A. Amann, Plenum, New York, 1980, pp. 69–129.

[30]Diwaka, R., and El Tahry, S. H., "Comparison of Computed Flow Fields and Wall Heat Fluxes with Measurements from Motored Reciprocating Engine-Like Geometries," *Computers in Engineering*, Vol. 1, edited by T. J. Cokonis, American Society of Mechanical Engineers, New York, 1983, pp. 175–188.

[31]Issa, R. I., "Solution of the Implicitly Discretized Fluid Flow Equations by Splitting of Operators," *Journal of Computational Physics*, Vol. 62, 1986, pp. 40–65.

[32]Rotta, J. C., "Statistische Theorie Nichthomoger Turbulanz. 1," *Zeitschrift fuer Physik*, Vol. 28, 1982, pp. 131–145.

[33]Pope, S. B., "An Improved Turbulent Mixing Model," *Combustion Science and Technology*, Vol. 28, 1982, pp. 131–145.

[34]Pope, S. B., and Gadh, R., "Fitting Noisy Data Using Cross-Validated Cubic Smoothing Splines," *Communications in Statistics-Simulation*, Vol. 17, No. 2, 1988, pp. 349–376.

[35]Haworth, D. C., "Developments in Applying a pdf/Monte Carlo Approach to Engine Cylinder Flows," GM Research Lab. Publ. GMR-5892, May 1987.

[36]Handscomb, D. C., and Hammersley, J. M., *Monte Carlo Methods*, Methuen, New York, 1965.

[37]Girimaji, S. S., and Pope, S. B., "A Stochastic Model for Velocity Gradients in Turbulence," *Physics of Fluids A*, Vol. 2, No. 2, 1990, pp. 242–256.

[38]Haworth, D. C., and Pope, S. B., "A Generalized Langevin Model for Turbulent Flows," *Physics of Fluids*, Vol. 29, No. 2, 1986, pp. 387–405.

## Notice to Authors

When submitting manuscripts to the *AIAA Journal*, please note the new address to which they should be mailed: Dr. George W. Sutton, Kaman Aerospace, 5055 East Broadway Boulevard, Suite C104, Tucson, AZ 85711.